

# Impact of GOLD Retrieved Thermospheric Temperatures on a Whole Atmosphere Data Assimilation Model

Fazlul I Laskar<sup>1</sup>, Nicholas Michael Pedatella<sup>2</sup>, Mihail V. Codrescu<sup>3</sup>, Richard Eastes<sup>4</sup>, Joseph S. Evans<sup>5</sup>, Alan G. Burns<sup>2</sup>, and William E. McClintock<sup>4</sup>

<sup>1</sup>Laboratory for Atmospheric and Space Physics, University of Colorado, Boulder, CO, USA

<sup>2</sup>National Center for Atmospheric Research (UCAR)

<sup>3</sup>NOAA-Space Weather Prediction Center

<sup>4</sup>Laboratory for Atmospheric and Space Physics

<sup>5</sup>Computational Physics, Incorporated

November 24, 2022

## Abstract

The present investigation evaluates the assimilation of synthetic data which has properties similar to actual Global-scale Observations of the Limb and Disk (GOLD) level-2 (L2) and other conventional lower atmospheric observations. The lower atmospheric and GOLD L2 temperature (Tdisk) are assimilated in the Whole Atmosphere Community Climate Model with thermosphere-ionosphere eXtension (WACCMX) using Data Assimilation Research Testbed (DART). It is found that inclusion of the GOLD Tdisk improves the forecast root mean square error (RMSE) and bias by 5% and 71%. When compared to lower atmosphere only assimilation the improvements in RMSE and bias are 20% and 94%. An investigation of the global DW1 and local diurnal tidal characteristics shows that inclusion of the GOLD temperatures improves the DW1 by about 8% and diurnal tide by more than 17%. The percentage improvement in tides is higher at lower thermospheric altitudes. Considerable improvements in the model state are also seen at times and locations where there are no GOLD observations available. These results and the background data assimilation procedure are presented here, which demonstrates that GOLD thermospheric temperature is an excellent dataset which can be used for thermospheric assimilation studies and operational purposes.

1                   **Impact of GOLD Retrieved Thermospheric**  
2                   **Temperatures on a Whole Atmosphere Data**  
3                   **Assimilation Model**

4                   **F. I. Laskar<sup>1</sup>, N. M. Pedatella<sup>2,3</sup>, M. V. Codrescu<sup>4</sup>, R. W. Eastes<sup>1</sup>, J. S.**  
5                   **Evans<sup>5</sup>, A. G. Burns<sup>2</sup>, W. McClintock<sup>1</sup>**

6                   <sup>1</sup>Laboratory for Atmospheric and Space Physics, University of Colorado, Boulder, CO, USA

7                   <sup>2</sup>High Altitude Observatory, National Center for Atmospheric Research, Boulder, CO, USA

8                   <sup>3</sup>COSMIC Program Office, University Center for Atmospheric Research, Boulder, CO, USA.

9                   <sup>4</sup>Space Weather Prediction Center, NOAA, Boulder, CO, USA

10                   <sup>5</sup>Computational Physics, Inc., Springfield, Virginia, USA

11                   **Key Points:**

- 12                   • Synthetic level 2 GOLD disk temperatures are assimilated and tested in WAC-
- 13                   CMX+DART
- 14                   • GOLD temperature assimilation improves the thermospheric temperature rmse
- 15                   and bias by 5-20% and 71-94%
- 16                   • DW1 and local diurnal tide are improved by about 7% and 17%, respectively at
- 17                   thermospheric altitudes.

## Abstract

The present investigation evaluates the assimilation of synthetic data which has properties similar to actual Global-scale Observations of the Limb and Disk (GOLD) level-2 (L2) and other conventional lower atmospheric observations. The lower atmospheric and GOLD L2 temperature ( $T_{disk}$ ) are assimilated in the Whole Atmosphere Community Climate Model with thermosphere-ionosphere eXtension (WACCMX) using Data Assimilation Research Testbed (DART). It is found that inclusion of the GOLD  $T_{disk}$  improves the forecast root mean square error (RMSE) and bias by 5% and 71%. When compared to lower atmosphere only assimilation the improvements in RMSE and bias are 20% and 94%. An investigation of the global DW1 and local diurnal tidal characteristics shows that inclusion of the GOLD temperatures improves the DW1 by about 8% and diurnal tide by more than 17%. The percentage improvement in tides is higher at lower thermospheric altitudes. Considerable improvements in the model state are also seen at times and locations where there are no GOLD observations available. These results and the background data assimilation procedure are presented here, which demonstrates that GOLD thermospheric temperature is an excellent dataset which can be used for thermospheric assimilation studies and operational purposes.

## Plain Language Summary

A perfect numerical model simulation of the Earth is the one that can reproduce the whole atmosphere-ionosphere-thermosphere (AIT) system at any point of time. With time, the numerical models are evolving and the simulation capabilities are enhanced with new understanding of the AIT system dynamics, but they are still far from perfect. On the other hand if one can measure any parameters or state of the AIT system at any point of time then the numerical models will be of no use. In the absence of both the above highly ambitious extreme possibilities, both the state of the art model capabilities and AIT measurements can be combined in a data assimilation framework to study the dynamics and to get a better understanding of AIT system. The present investigation evaluates GOLD mission level-2 disk temperatures and found that they can improve the thermospheric assimilation capability significantly.

## 1 Introduction

The upper atmosphere, above about 100 km, of the Earth is influenced by wave forcing from the lower atmosphere and by external solar and geomagnetic forcings. For a better understanding of the whole atmosphere comprising of atmosphere-ionosphere-thermosphere (AIT) system it is necessary to study and characterize the local and global variations. Ground based datasets have good local time coverage but they lack global coverage. While low-earth orbiting (LEO) satellite based measurements have good global coverage but they lack local time coverage. However, imaging measurements from a geostationary orbit can cover a great spatial and temporal window over a part of the globe. The recently launched Global-scale Observations of the Limb and Disk (GOLD) mission provides one such opportunity to image the Earth's thermosphere at an unprecedented spectral, spatial, and temporal resolution (Eastes et al., 2020; McClintock et al., 2020; Laskar et al., 2020). GOLD scans the Earth's disk from geostationary orbit for about 18.5 hours a day, from 0610 UT to 0040 UT. The daylight measurements of the nitrogen ( $N_2$ ) Lyman-Birge-Hopfield (LBH) bands in far-ultra-violet (FUV) can be used to retrieve thermospheric temperature over about, at times, one fourth of the globe (Eastes et al., 2020). With the availability of such partly global thermospheric dataset and other local plus global observations at different altitudes of the atmosphere an investigation of the AIT system is warranted by re-analyzing all these measurements.

The primary measurements from GOLD mission are FUV emissions, which can be used in the data assimilation models (Cantrall et al., 2019). But in the present inves-

68 tigation the thermospheric temperatures that are retrieved from the N<sub>2</sub> LBH bands are  
 69 assimilated. This is because the temperatures retrieved from GOLD LBH band emis-  
 70 sions are validated regularly and such retrievals have a long history (Aksnes et al., 2006;  
 71 Krywonos et al., 2012; Meier et al., 2015). Moreover, investigations from a forward mod-  
 72 eling study showed that model underestimate the radiance compared to GOLD obser-  
 73 vations (Greer et al., 2020).

74 The thermosphere-ionosphere (TI) system can change very rapidly with the change  
 75 of external forcings. Also the lower atmospheric wave forcings influence the TI system  
 76 significantly. So, a whole AIT data assimilation would be of great resource for the in-  
 77 vestigation of TI system (Jackson et al., 2019). Most of the earlier assimilation systems  
 78 assimilated the lower atmosphere (below  $\sim 100$  km ) data (Pedatella et al., 2014; McCor-  
 79 mack et al., 2017) or used thermosphere-ionosphere models having a lower boundary be-  
 80 tween 80 km and 100 km altitudes (M. V. Codrescu et al., 2004; Lee et al., 2012; Chartier  
 81 et al., 2016; Chen et al., 2017; Rajesh et al., 2017; S. M. Codrescu et al., 2018; Sutton,  
 82 2018; Cantrall et al., 2019; He et al., 2019).

83 Assimilation experiments using whole atmosphere models have also been performed  
 84 (Wang et al., 2011; Pedatella et al., 2018), but they assimilated only the lower and mid-  
 85 dle atmosphere observations from altitudes below about 100 km. The present investi-  
 86 gation aims to evaluate the impact of GOLD mission level-2 thermospheric disk temper-  
 87 atures on a whole AIT data assimilation model, where both lower atmosphere and ther-  
 88 mosphere data are assimilated.

## 89 2 Model, Data, and Methodology

90 The main objective of this study is to assimilate and assess the impact of the GOLD  
 91 disk temperatures ( $T_{disk}$ ) observations in a whole atmosphere model, for that we have  
 92 used the Whole Atmosphere Community Climate Model with thermosphere-ionosphere  
 93 eXtension (WACCMX). Data assimilation is implemented using the Data Assimilation  
 94 Research Testbed (DART) ensemble Kalman filter. Details about the model and obser-  
 95 vations are given below.

### 96 2.1 WACCMX+DART

97 The recently developed WACCMX version 2.1 is a whole atmosphere general cir-  
 98 culation model extending from the surface to the upper thermosphere ( 500-700 km de-  
 99 pending on solar activity) (Liu et al., 2018). WACCMX includes the chemical, dynam-  
 100 ical, and physical processes that are necessary to model the lower, middle, and upper at-  
 101 mospheres. The thermosphere and ionosphere processes are similar to those in the NCAR  
 102 Thermosphere-Ionosphere-Electrodynamics General Circulation Model (TIE-GCM), in-  
 103 cluding the transport of O<sup>+</sup> and self-consistent electrodynamics as well as realistic so-  
 104 lar and geomagnetic forcing. The model horizontal resolution is  $1.9^\circ \times 2.5^\circ$  in latitude  
 105 and longitude, and the vertical resolution is 0.25 scale heights above  $\sim 50$  km.

106 To reproduce specific events in WACCMX it is necessary to constrain the model  
 107 meteorology (i.e., dynamics). The data assimilation capability in WACCMX was initially  
 108 implemented by Pedatella et al. (2018) using DART (Anderson et al., 2009), which uses  
 109 the ensemble Kalman filter. But the earlier adoption was limited to assimilation of ob-  
 110 servations at altitudes below 100 km. In the present investigation the WACCMX+DART  
 111 assimilation capability has been extended to thermosphere altitudes for the assimilation  
 112 of GOLD L2  $T_{disk}$ . As the thermospheric dynamics can change fast in response to changes  
 113 in forcing conditions, we use 1 hour assimilation frequency.

114 An essential part of ensemble data assimilation is that the ensemble members should  
 115 have sufficient spread. To increase the spread in the ensemble members we use variable

external forcing parameters with standard deviations of 15 sfu and 1 in F10.7 solar flux and Kp index over the ensemble members. For the assessment of the impact of assimilating GOLD T<sub>disk</sub> data we run two Observing System Simulation Experiments (OSSEs); one with synthetic observations for altitudes below about 100 km, we call it lower atmosphere only (LA) and second one is with synthetic observations from lower atmosphere plus GOLD L2 T<sub>disk</sub> (LA+GOLD) observations. These synthetic observations are generated based on a true or reference state from a free run of WACCMX. A random error is applied to the synthetic observations based on the errors in the actual observations.

For the present OSSEs the lower atmosphere observations include conventional meteorological observations (i.e., aircraft temperatures, radiosonde temperatures, and winds), Global Positioning System (GPS) radio occultation refractivity, and temperature observations from Thermosphere Ionosphere Mesosphere Energetics Dynamics (TIMED) satellite Sounding of the Atmosphere using Broadband Emission Radiometry (SABER) instrument and Aura Microwave Limb Sounder (MLS). The solar and geomagnetic forcing parameters for the true state is F10.7=76 sfu and Kp=0. While for the OSSEs the F10.7 has an ensemble mean value of 100 sfu and a spread of 15 sfu, resetting any F10.7 value less than 60 sfu to 60 sfu. Similarly, Kp index values have a mean of 0.33 with a spread of 1, but minimum Kp value was restricted to 0. Based on recommendations from previous studies (e.g., Pedatella et al., 2014, 2018) and to reduce the computational load we employ 40 member ensembles for both the OSSEs.

## 2.2 Assimilation of GOLD T<sub>disk</sub> in WACCMX+DART

The daytime N<sub>2</sub> LBH bands can be used to retrieve lower thermospheric temperatures (Aksnes et al., 2006; Krywonos et al., 2012; Meier et al., 2015), which are publicly available in the GOLD web-page <https://gold.cs.ucf.edu/>. Figure 1 shows an example disk image of the retrieved temperatures from GOLD daytime disk observations (Figure 1a), their random uncertainty (Figure 1b), and a map of solar zenith angle variation over the disk (Figure 1c). A higher uncertainty in temperatures can be seen in the Northern hemisphere, which is due to low signal to noise ratio (SNR) corresponding to higher solar zenith angles (SZAs) measurements. Temperatures like these are retrieved from 1x1 pixel binned level 1C (L1C) LBH radiance data, so the noise level is high. In a future release the L1C data will be binned at 2x2 pixels to retrieve the disk temperatures, which will reduce the noise by about a factor of 7 (Eastes et al., 2020). Though the temperature data in 1x1 L1C pixel binning are noisy there are lot of geophysical variations in them, which are very clear in 2x2 L1C-pixel binning as can be seen in Eastes et al. (2020) or when some of the noisy data are filtered out (not shown here). So, to create a set of synthetic data for the current investigation, we have reduced the random uncertainty in the currently available operational data by 7 times.

The daytime N<sub>2</sub> LBH band emissions emanates primarily from the lower thermosphere. The altitude profiles of variation of 136.5 nm LBH band normalized contribution function for some representative solar zenith angles are shown in Figure 2(a). A contribution function provides information about the altitudes from where the emission emanated from. It can be noted that until about 55 degrees SZA the contribution function has nearly similar shape and the peak altitude varies by about 10 km. A plot of the 0° SZA contribution function and its mathematical function fit in log(*p/p*<sub>o</sub>) coordinate, where *p* and *p*<sub>o</sub> are pressures at a given level and at the surface, respectively, is shown in Figure 2(b). As DART uses log(*p/p*<sub>o</sub>) as vertical coordinate, we use such logarithmic scale in the forward operator calculations. The mathematical function used in the fit is a log normal function of the form:

$$CF_{fit} = (A/x)e^{-\frac{(\log_{10}(-x)-\mu)^2}{2\sigma^2}} \quad (1)$$

Where, *A*, *μ*, *σ* are amplitude, mean and standard deviation of *x*, the actual contribution function. This function is used as the forward operator which translates the model

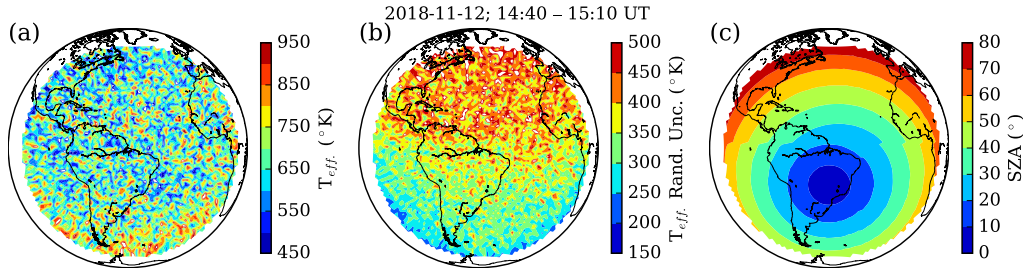


**Figure 1.** An example disk temperature image retrieved from GOLD daytime LBH disk observations (a), the random uncertainty (b), and a map of solar zenith angle variation over the disk are shown. Higher uncertainties in the Northern hemisphere are due to higher solar zenith angle and thus relatively lower signal to noise ratio measurements.

166 state to what would be observed by GOLD. Since GOLD observes airglow layer integrated  
 167 emissions, which are used for the temperature retrieval, the forward operator weights the  
 168 model temperature profiles to estimate a GOLD equivalent effective temperature.

169 **2.3 Localization of the impact of GOLD observations**

170 GOLD is capable of observing day-time Earth’s disk temperatures centered over  
 171 American longitudes, which are representative of the whole LBH emission layer as shown  
 172 by the contribution functions in Figure 2. To avoid any spurious correlation at altitudes  
 173 and locations far away from the observation point, the observations are localized in space  
 174 so that there is no direct impact at far away locations. A plot of the variation of covari-  
 175 ance vertical localization factor is shown in Figure 3. The peak of the vertical localiza-  
 176 tion profile is close to the peak of the contribution function, which is about 160 km (or  
 177  $10^{-5}$  hPa or -20 in  $\log(p/p_0)$  coordinate). As the thermosphere maintains an isother-  
 178 mal state, a change in temperature at the peak altitude is expected to have a positive  
 179 correlation at all altitudes in the thermosphere. Due to this characteristics of the ther-  
 180 mosphere the localization function is chosen to be positive at upper thermosphere, even  
 181 though the contribution function is near zero at those altitudes. The horizontal local-  
 182 ization used is standard Gaspari-Cohn type (Gaspari & Cohn, 1999; Anderson & Lei,  
 183 2013) with a half width of 0.2 radians.

184 **3 Results and Discussion**

185 For the present OSSE investigation we test the assimilation of GOLD  $T_{disk}$  obser-  
 186 vations in WACCMX+DART for 9-13 November 2018, where the assimilation experi-  
 187 ments started from 20 October 2018. Figure 4 shows an example of True (a), synthetic  
 188 (c), forecast (b), and analysis (d) of GOLD disk temperatures on 13 November 2018 at  
 189 15 UT. It can be noted that the synthetic data used in these assimilations have spatial  
 190 properties similar to those shown in Figure 1(a). The analysis states are obtained by as-  
 191 simulating the synthetic data in WACCMX+DART. The analysis state compares very  
 192 well with the True state, which indicate that the data assimilation system performs well.  
 193 Further diagnosis of the OSSEs are discussed below. It may be noted here that in the  
 194 assimilation setup the  $T_{disk}$  observations only directly impact temperatures in WAC-  
 195 CMX+DART.

196 Further diagnosis of the assimilation is performed by calculating root mean square  
 197 error (RMSE) and bias between model (forecast and analysis) and  $T_{disk}$  observations.  
 198 Figure 5 shows the variation of the RMSE (5a) and bias (5b) for the LA only analysis

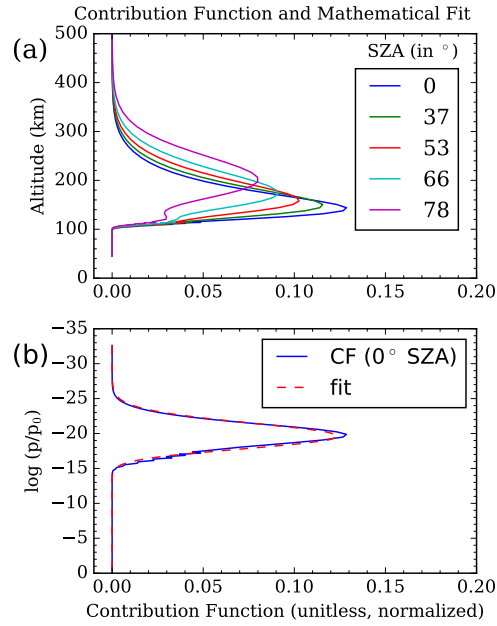


**Figure 2.** Variation of 136.5 nm LBH band contribution function for representative solar zenith angles (a). It can be noted that until about 60° SZA the contribution function has similar shape and does not differ much. A plot of the 0° SZA contribution function and its mathematical function fit in  $\log(p/p_0)$  coordinate (b) that is used in the forward operator.

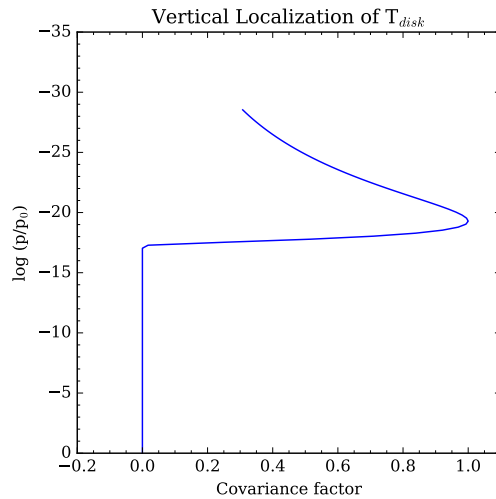


**Figure 3.** Variation of covariance localization factor with altitude. The peak of the vertical localization profile is close to the peak of the contribution function, which is about -20 (about 160 km or  $10^{-5}$  hPa).

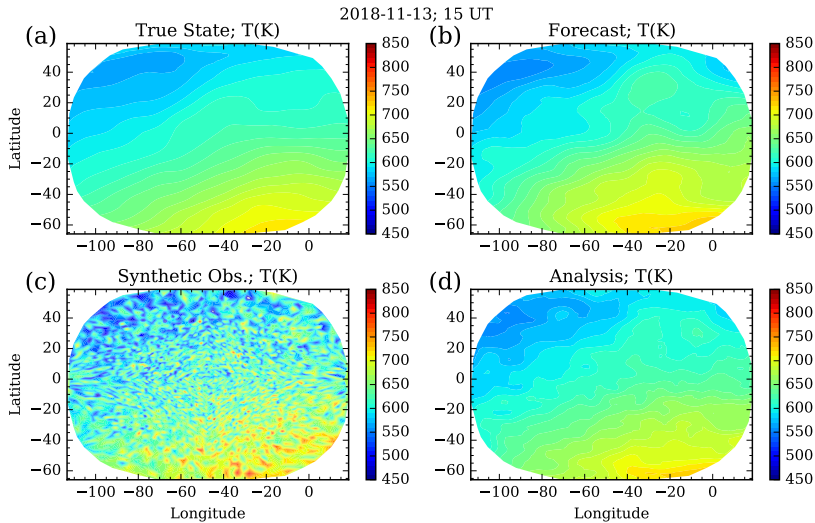


**Figure 4.** True (a), forecast (b), synthetic (c), and analysis (d) disk temperature states. It can be noted that the synthetic data used in this assimilation has spatial properties similar to those shown in Figure 1(a). The analysis state compares very well with the True state.

199 (LA anal.), LA+GOLD forecast (LA+GOLD fore.), and LA+GOLD analysis (LA+GOLD  
 200 anal.). Significant improvement in LA+GOLD assimilated forecast RMSE and bias can  
 201 be seen, which are about 5% and 71%. A dramatic improvement in LA only assimi-  
 202 lation RMSE and bias are observed which are about 20% and 94%. It is also apparent in  
 203 Figure 5 that the short-term forecast in the LA+GOLD experiment is improved rela-  
 204 tive to the LA experiment. This demonstrates the effectiveness of the assimilation, and  
 205 shows that the assimilation of GOLD temperatures can improve short-term forecast of  
 206 the thermosphere.

207 Figure 6 shows a comparison of the whole atmosphere temperature profiles from  
 208 true state, LA only assimilation, and LA+GOLD assimilation for 14 UT (left column)  
 209 and 18 UT (right column) at different locations inside the GOLD’s field of view. Though  
 210 there are differences between the true state and the analysis state in the LA+GOLD ex-  
 211 periment, the differences are lower compared to the LA only experiment. It may be noted  
 212 that the average solar forcing for the assimilation experiments is about 25 sfu higher com-  
 213 pared to the true state solar forcing. Significant improvements are also observed (not shown  
 214 here but another representation is shown later) at all hours from 7 -23 UT, where data  
 215 are available from the GOLD disk observations. The zonal mean (ZM) temperature pro-  
 216 files (lower panels in Figure 6) also show significant improvement compared to LA only  
 217 assimilation. These improvements in the analysis state suggests that GOLD  $T_{disk}$  im-  
 218 proves the model state significantly.

219 The results in Figure 6 were for sample times and locations within the GOLD’s ob-  
 220 serving temporal and spatial windows. Whereas, in Figure 7, we show a similar compar-  
 221 ison as that in Figure 6 but at locations outside GOLD’s field of view, to see its impact.  
 222 Figure 7(a) and (b) show comparison at 2 UT and 15 UT and over (65°N, 60°W) where  
 223 there are no or very little observations from GOLD. Even then one can note some im-  
 224 provement in the LA+GOLD analysis state compared to LA analysis. While in Figure  
 225 7(c) and (d) the same 2 UT and 15 UT are shown but at the other side of the hemisphere  
 226 at (0°S, 120°E). As there are no observations from GOLD over those locations, the im-  
 227 provements compared to LA analysis is very small. This improvement in the LA+GOLD  
 228 analysis outside the GOLD’s field of view suggests that there are indirect improvement

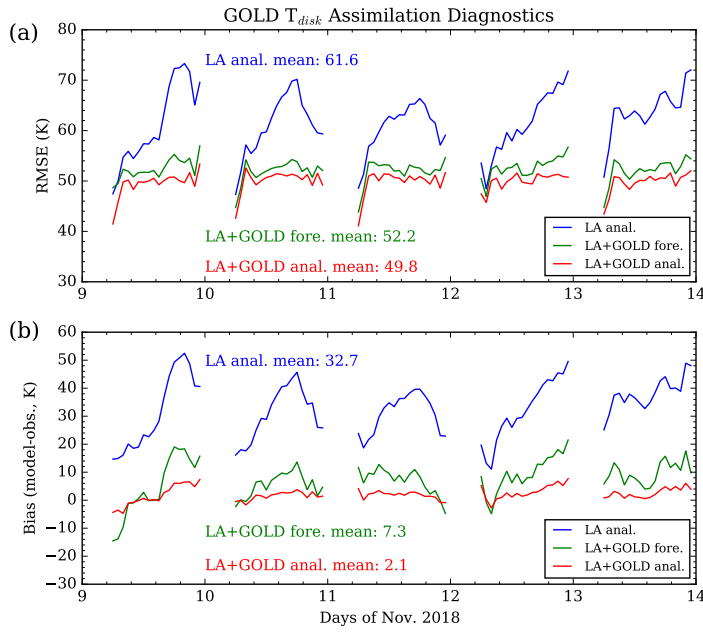


**Figure 5.** Diagnostics of the assimilation performed using lower atmosphere plus GOLD data are compared with lower atmosphere only assimilation. RMSE (a) and bias (b) for the LA analysis (LA anal.), LA+GOLD forecast (LA+GOLD fore.), and LA+GOLD analysis (LA+GOLD anal.). Significant improvement in LA+GOLD analysis RMSE and bias can be seen which are about 5% and 71%, compared to LA+GOLD forecast state. When compared to LA only assimilation the improvement in RMSE and bias are about 20% and 94%.

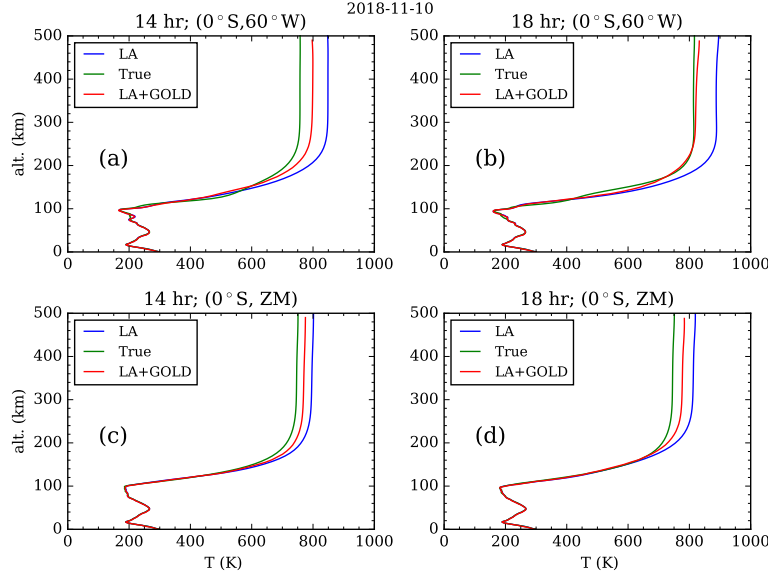


**Figure 6.** Comparison of the whole atmosphere temperature profiles from true state, lower atmosphere only assimilation (LA), and lower-atmosphere plus GOLD assimilation (LA+GOLD) for 14 UT (left column) and 18 UT (right column) at different locations inside the GOLD field of view. The zonal mean (ZM) in LA+GOLD also shows significant improvement compared to LA only assimilation.

229 in terms of the adjustment in the model forecast capability. Thus one can say that the  
 230 assimilation of GOLD  $T_{disk}$  data improves the model state globally, but the impact is  
 231 lower at locations and times outside GOLD’s window of observations.

232 In Figure 8 we present a global picture of the impact of GOLD assimilation on model  
 233 temperatures at a particular pressure level ( $7.3 \times 10^{-7}$  hPa, about 194 km) but over the  
 234 equator for the 5-days of OSSEs in November 2018. We show the difference between true  
 235 state and the LA only assimilation ( $T_{LA} - T_{true}$ ) in (a). While Figure 8(b) shows temper-  
 236 ature difference between LA+GOLD experiment and true state ( $T_{LA+GOLD} - T_{true}$ )  
 237 at that pressure. It can be seen that overall the differences are smaller in Figure 8(b)  
 238 compared to Figure 8(a). Also, the  $T_{LA+GOLD} - T_{true}$  differences are very near to zero  
 239 at second half of UT times of the day and within  $110^\circ\text{W}$  to  $20^\circ\text{E}$  longitudes through 0,  
 240 where GOLD disk data are mostly available. There are some enhanced negative occur-  
 241 rences in  $\Delta T$  within the  $110^\circ\text{W}$  to  $20^\circ\text{E}$  longitude (in Figure 8b), which are mostly in  
 242 the night-sector where there are few or no observations from GOLD. One can see an en-  
 243 hanced region of temperature that is propagating with time along longitude, which is  
 244 the signature of diurnal westward propagating wave number 1 (DW1) tide, character-  
 245 ization of such tides are given below.

246 We have observed above that DW1 like waves in temperatures are seen in Figure  
 247 8. Here we show the comparison of DW1 amplitudes between true, LA experiment, and  
 248 LA+GOLD experiment in Figure 9(a). The DW1 amplitude is highest for the LA ex-  
 249 periment and compared to it the LA+GOLD experiment DW1 has amplitudes closer to  
 250 the true state. The percentage improvement in LA+GOLD experiment DW1 and per-  
 251 centage difference from true state are shown in Figure 9(b). The percentage improve-  
 252 ments are higher than 7% at all the altitudes above about 130 km. Higher than 10% am-  
 253 plitudes are also observed in percentage improvement at altitudes below 150 km, which  
 254 are mainly due to the lower values of true state DW1 tide in temperature. Though there

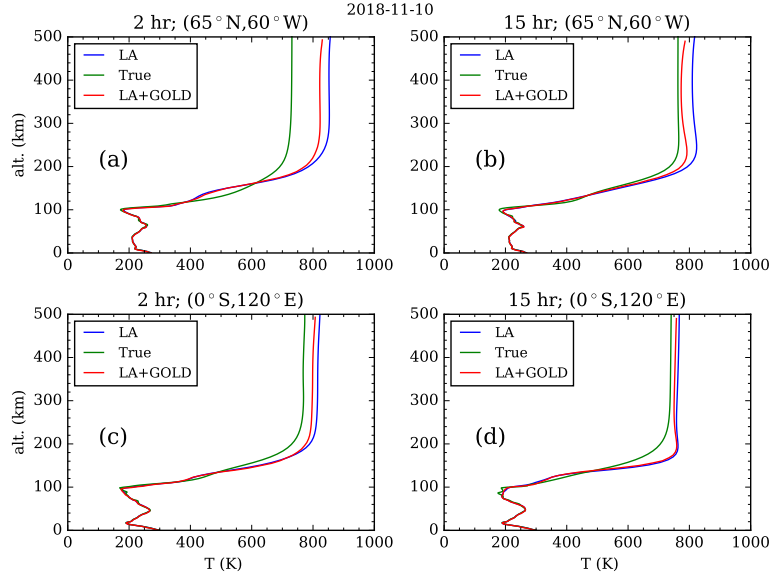


**Figure 7.** Comparison of the whole atmosphere temperature profiles between true state, lower atmosphere only assimilation (LA), and lower-atmosphere plus GOLD assimilation (LA+GOLD) for 2 UT (left column) and 14 UT (right column) at different locations outside the GOLD’s field of view. Significant improvements are observed, even, at locations and times where there are no GOLD data.

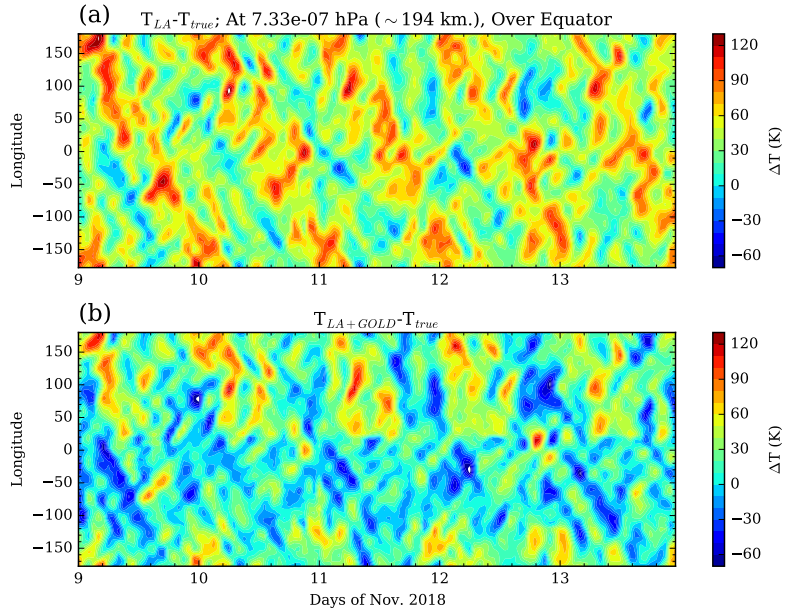


**Figure 8.** Longitudinal variation of the difference between true state and the lower atmosphere only assimilation ( $T_{LA}-T_{true}$ , in a) and true state and LA+GOLD assimilation ( $T_{LA+GOLD}-T_{true}$ , in b) are shown for the 5 days during November. It can be seen that the differences (in b) are very near zero at second half of UT days and at locations (110°W to 20°E, through 0°), where GOLD data are mostly available.

255 are more than 7% improvements in DW1 after assimilation of GOLD  $T_{disk}$ , there is still  
 256 about 27% (about  $10^{\circ}\text{K}$ ) difference between true and the GOLD assimilated DW1. This  
 257 discrepancy could be attributed to GOLD only observing about one fourth of the globe  
 258 for a portion of the day, so the improvement in the global DW1 tide is limited. But lo-  
 259 cally over American longitudes the improvement could be better which is discussed be-  
 260 low.

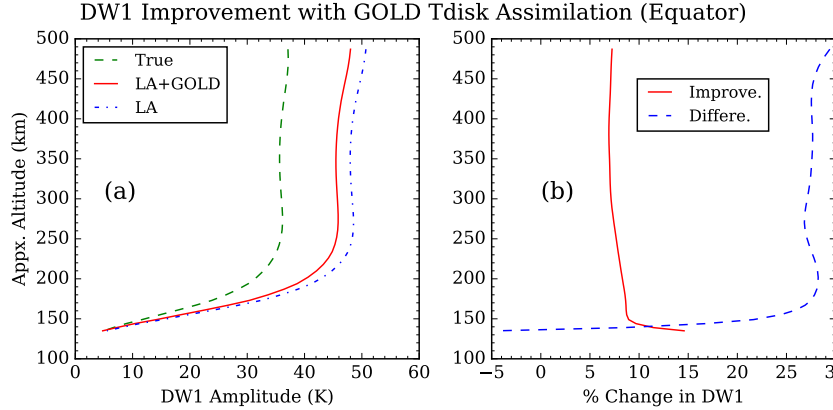


**Figure 9.** Improvement of DW1 amplitude as compared to LA assimilation experiment. Altitude variation of DW1 (a) of true (dashed), LA+GOLD (solid), and LA (dash-dotted) are shown. Percentage difference (dashed) and improvement (solid) in DW1 amplitudes (b) compared to true and lower atmosphere only assimilation DW1 amplitudes are also shown.

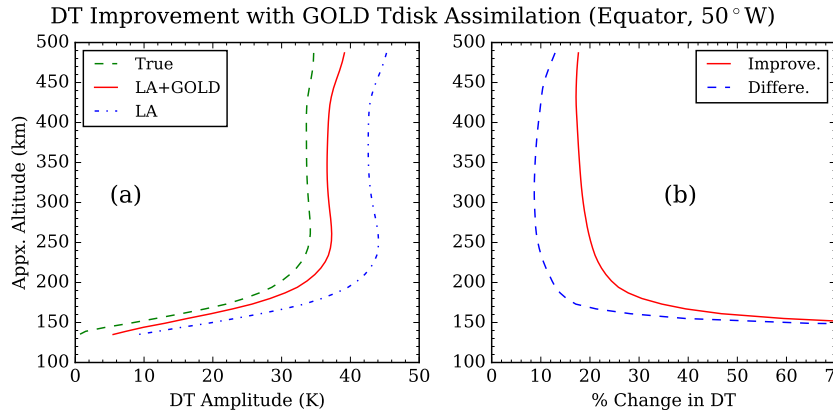


**Figure 10.** Improvement of local diurnal tidal (DT) amplitude as compared to LA only assimilation. Altitude variation of DT (a) of true (dashed), LA+GOLD (solid), and LA (dash-dotted) are shown. Percentage difference (dashed) and improvement (solid) in DT amplitudes (b) compared to true and lower atmosphere only assimilation DT amplitudes are also shown.

261 To investigate the local tides over the Americas we have done a similar analysis as  
 262 that in Figure 9, but for the local diurnal tide (DT, at  $0^{\circ}$ ,  $50^{\circ}\text{W}$ ), which is shown in Fig-  
 263 ure 10. Here it can be seen that the LA+GOLD experiment DT amplitude profile is much  
 264 closer to true state compared to LA experiment. Also, the improvements are more than  
 265 17% compared to LA assimilation and difference between true and LA+GOLD DT is

266 less than 10% at thermospheric levels. As the local tide estimation is affected by inter-  
 267 action between global and local components (Laskar et al., 2016) the discrepancies could  
 268 be attributed to difference between global components of all the three states.

## 269 4 Conclusions

270 A set of synthetic observation from troposphere to thermosphere are used in this  
 271 investigation to evaluate the impact of GOLD Level-2 disk temperature measurements  
 272 to improve the thermospheric data assimilation and dynamics. Following are the salient  
 273 findings of this investigation:

- 274 1. Assimilation of GOLD disk temperatures improves the themospheric assimilation  
 275 over the GOLD field of view and also globally to some extent.
- 276 2. The model forecast RMSE and bias are improved by 5% and 71%, and the improve-  
 277 ments are 20% and 94% when compared with lower atmosphere only assimilation.  
 278 Thus, the inclusion of GOLD  $T_{disk}$  in the assimilation improves the short term  
 279 forecast of the thermosphere.
- 280 3. The global diurnal tide of wavenumber 1 (DW1) and local diurnal tide over Amer-  
 281 icas improve by about 8% and by more than 17%, respectively upon assimilation  
 282 of GOLD temperatures.
- 283 4. Though GOLD observations are available only during day-light hours, it improves  
 284 the night time state too.

285 These results demonstrate that GOLD level 2 disk temperatures are an excellent  
 286 set of observations, which will be of use in the future investigations of atmospheric cou-  
 287 pling, dynamics, and operational use. As the GOLD  $T_{disk}$  assimilation improves ther-  
 288 mosphere, the current investigation shows a promise towards better forecast capability  
 289 of space weather.

## 290 Acknowledgments

291 This research was supported by NASA Contract 80GSFC18C0061 to the University of  
 292 Colorado, Boulder. This material is also based upon work supported by the National Cen-  
 293 ter for Atmospheric Research (NCAR), which is a major facility sponsored by the Na-  
 294 tional Science Foundation under Cooperative Agreement No. 1852977. Computing and  
 295 data storage resources, including the Cheyenne supercomputer (doi:10.5065/D6RX99HX),  
 296 were provided by the Computational and Information Systems Laboratory (CISL) at NCAR.  
 297 WACCMX is part of the Community Earth System Model (CESM) and the source code  
 298 is available at <http://www.cesm.ucar.edu>. DART is available at [https://www.image](https://www.image.ucar.edu/DAReS/DART/)  
 299 [.ucar.edu/DAReS/DART/](https://www.image.ucar.edu/DAReS/DART/). The Level 2 data used in this study are available at the GOLD  
 300 Science Data Center (<http://gold.cs.ucf.edu/search/>) and at NASA's Space Physics  
 301 Data Facility (<https://spdf.gsfc.nasa.gov/pub/data/gold/>).

## 302 References

- 303 Aksnes, A., Eastes, R., Budzien, S., & Dymond, K. (2006). Neutral temperatures  
 304 in the lower thermosphere from  $N_2$  Lyman-Birge-Hopfield (LBH) band profiles.  
 305 *Geophysical Research Letters*, *33*(15). doi: 10.1029/2006gl026255
- 306 Anderson, J., Hoar, T., Raeder, K., Liu, H., Collins, N., Torn, R., & Avellano, A.  
 307 (2009, September). The data assimilation research testbed: A community fa-  
 308 cility. *Bulletin of the American Meteorological Society*, *90*(9), 1283–1296. doi:  
 309 10.1175/2009bams2618.1
- 310 Anderson, J., & Lei, L. (2013, October). Empirical localization of observation im-  
 311 pact in ensemble kalman filters. *Monthly Weather Review*, *141*(11), 4140–4153.  
 312 doi: 10.1175/mwr-d-12-00330.1

- 313 Cantrall, C. E., Matsuo, T., & Solomon, S. C. (2019, October). Upper atmosphere  
314 radiance data assimilation: A feasibility study for GOLD far ultraviolet obser-  
315 vations. *Journal of Geophysical Research: Space Physics*, *124*(10), 8154–8164.  
316 doi: 10.1029/2019ja026910
- 317 Chartier, A. T., Matsuo, T., Anderson, J. L., Collins, N., Hoar, T. J., Lu, G., ...  
318 Bust, G. S. (2016, January). Ionospheric data assimilation and forecasting dur-  
319 ing storms. *Journal of Geophysical Research: Space Physics*, *121*(1), 764–778.  
320 doi: 10.1002/2014ja020799
- 321 Chen, C.-H., Lin, C., Chen, W.-H., & Matsuo, T. (2017, February). Modeling  
322 the ionospheric prereversal enhancement by using coupled thermosphere-  
323 ionosphere data assimilation. *Geophysical Research Letters*, *44*(4), 1652–1659.  
324 doi: 10.1002/2016gl071812
- 325 Codrescu, M. V., Fuller-Rowell, T. J., & Minter, C. F. (2004, November). An  
326 ensemble-type kalman filter for neutral thermospheric composition dur-  
327 ing geomagnetic storms. *Space Weather*, *2*(11), n/a–n/a. doi: 10.1029/  
328 2004sw000088
- 329 Codrescu, S. M., Codrescu, M. V., & Fedrizzi, M. (2018, January). An ensemble  
330 kalman filter for the thermosphere-ionosphere. *Space Weather*, *16*(1), 57–68.  
331 doi: 10.1002/2017sw001752
- 332 Eastes, R. W., McClintock, W. E., Burns, A. G., Anderson, D. N., Andersson, L.,  
333 Aryal, S., ... Woods, T. N. (2020). Initial observations by the gold mission.  
334 *Journal of Geophysical Research: Space Physics*, *125*(7), e2020JA027823. doi:  
335 10.1029/2020JA027823
- 336 Gaspari, G., & Cohn, S. E. (1999, January). Construction of correlation functions in  
337 two and three dimensions. *Quarterly Journal of the Royal Meteorological Soci-  
338 ety*, *125*(554), 723–757. doi: 10.1002/qj.49712555417
- 339 Greer, K. R., Eastes, R., Solomon, S., McClintock, W., Burns, A., & Rusch, D.  
340 (2020, June). Variations of lower thermospheric FUV emissions based on  
341 GOLD observations and GLOW modeling. *Journal of Geophysical Research:  
342 Space Physics*, *125*(6). doi: 10.1029/2020ja027810
- 343 He, J., Yue, X., Wang, W., & Wan, W. (2019, August). EnKF ionosphere and ther-  
344 mosphere data assimilation algorithm through a sparse matrix method. *Jour-  
345 nal of Geophysical Research: Space Physics*, *124*(8), 7356–7365. doi: 10.1029/  
346 2019ja026554
- 347 Jackson, D. R., Fuller-Rowell, T. J., Griffin, D. J., Griffith, M. J., Kelly, C. W.,  
348 Marsh, D. R., & Walach, M.-T. (2019, September). Future directions for whole  
349 atmosphere modeling: Developments in the context of space weather. *Space  
350 Weather*, *17*(9), 1342–1350. doi: 10.1029/2019sw002267
- 351 Krywonos, A., Murray, D. J., Eastes, R. W., Aksnes, A., Budzien, S. A., & Daniell,  
352 R. E. (2012, September). Remote sensing of neutral temperatures in the  
353 Earth’s thermosphere using the Lyman-Birge-Hopfield bands of N<sub>2</sub>: Compar-  
354 isons with satellite drag data. *Journal of Geophysical Research: Space Physics*,  
355 *117*(A9). doi: 10.1029/2011ja017226
- 356 Laskar, F. I., Chau, J. L., Stober, G., Hoffmann, P., Hall, C. M., & Tsutsumi,  
357 M. (2016, May). Quasi-biennial oscillation modulation of the middle-  
358 and high-latitude mesospheric semidiurnal tides during august-september.  
359 *Journal of Geophysical Research: Space Physics*, *121*(5), 4869–4879. doi:  
360 10.1002/2015ja022065
- 361 Laskar, F. I., Eastes, R. W., Martinis, C. R., Daniell, R. E., Pedatella, N. M., Burns,  
362 A. G., ... Codrescu, M. V. (2020, July). Early morning equatorial ionization  
363 anomaly from GOLD observations. *Journal of Geophysical Research: Space  
364 Physics*, *125*(7). doi: 10.1029/2019ja027487
- 365 Lee, I. T., Matsuo, T., Richmond, A. D., Liu, J. Y., Wang, W., Lin, C. H., ...  
366 Chen, M. Q. (2012, October). Assimilation of FORMOSAT-3/COSMIC  
367 electron density profiles into a coupled thermosphere/ionosphere model using

- 368 ensemble kalman filtering. *Journal of Geophysical Research: Space Physics*,  
 369 *117*(A10), n/a–n/a. doi: 10.1029/2012ja017700
- 370 Liu, H.-L., Bardeen, C. G., Foster, B. T., Lauritzen, P., Liu, J., Lu, G., . . . Wang,  
 371 W. (2018). Development and validation of the whole atmosphere commu-  
 372 nity climate model with thermosphere and ionosphere extension (waccm-x  
 373 2.0). *Journal of Advances in Modeling Earth Systems*, *10*(2), 381–402. doi:  
 374 10.1002/2017MS001232
- 375 McClintock, W. E., Eastes, R. W., Beland, S., Bryant, K. B., Burns, A. G., Cor-  
 376 reira, J., . . . Veibel, V. (2020, May). Global-scale observations of the limb  
 377 and disk mission implementation: 2. observations, data pipeline, and level 1  
 378 data products. *Journal of Geophysical Research: Space Physics*, *125*(5). doi:  
 379 10.1029/2020ja027809
- 380 McCormack, J., Hoppel, K., Kuhl, D., de Wit, R., Stober, G., Espy, P., . . . Hibbins,  
 381 R. (2017, February). Comparison of mesospheric winds from a high-altitude  
 382 meteorological analysis system and meteor radar observations during the  
 383 boreal winters of 2009–2010 and 2012–2013. *Journal of Atmospheric and*  
 384 *Solar-Terrestrial Physics*, *154*, 132–166. doi: 10.1016/j.jastp.2016.12.007
- 385 Meier, R. R., Picone, J. M., Drob, D., Bishop, J., Emmert, J. T., Lean, J. L.,  
 386 . . . Gibson, S. T. (2015, January). Remote sensing of earth’s limb by  
 387 TIMED/GUVI: Retrieval of thermospheric composition and temperature.  
 388 *Earth and Space Science*, *2*(1), 1–37. doi: 10.1002/2014ea000035
- 389 Pedatella, N. M., Liu, H.-L., Marsh, D. R., Raeder, K., Anderson, J. L., Chau, J. L.,  
 390 . . . Siddiqui, T. A. (2018). Analysis and hindcast experiments of the 2009  
 391 sudden stratospheric warming in WACCMX+DART. *J. Geophys. Res.: Space*  
 392 *Physics*, *123*(4), 3131–3153. doi: 10.1002/2017JA025107
- 393 Pedatella, N. M., Raeder, K., Anderson, J. L., & Liu, H.-L. (2014). Ensemble data  
 394 assimilation in the whole atmosphere community climate model. *J. Geophys.*  
 395 *Res.: Atmospheres*, *119*(16), 9793–9809. doi: 10.1002/2014jd021776
- 396 Rajesh, P. K., Lin, C. H., Chen, C. H., Lin, J. T., Matsuo, T., Chou, M. Y., . . .  
 397 You, C. F. (2017, September). Equatorial plasma bubble generation inhibition  
 398 during 2015 st. patrick’s day storm. *Space Weather*, *15*(9), 1141–1150. doi:  
 399 10.1002/2017sw001641
- 400 Sutton, E. K. (2018, June). A new method of physics-based data assimilation for  
 401 the quiet and disturbed thermosphere. *Space Weather*, *16*(6), 736–753. doi: 10  
 402 .1002/2017sw001785
- 403 Wang, H., Fuller-Rowell, T. J., Akmaev, R. A., Hu, M., Kleist, D. T., & Iredell,  
 404 M. D. (2011, December). First simulations with a whole atmosphere data  
 405 assimilation and forecast system: The january 2009 major sudden stratospheric  
 406 warming. *Journal of Geophysical Research: Space Physics*, *116*(A12), n/a–n/a.  
 407 doi: 10.1029/2011ja017081